Molecular Cancer Therapeutics

Mouse Strains Influence Clearance and Efficacy of Antibody and Antibody–Drug Conjugate Via Fc–FcγR Interaction

Fu Li[1], Michelle L. Ulrich[1], Vincent Feng-Sheng Shih[2], Julia H. Cochran[1], Joshua H. Hunter[1], Lori Westendorf[1], Jason Neale[2], and Dennis R. Benjamin[1]

Abstract

To provide a better understanding of the pharmacokinetics–pharmacodynamics relationships of antibody-based drugs, we analyzed several chimeric and humanized monoclonal antibodies or antibody–drug conjugates (ADC) for PK and efficacy among four strains of mice. Notably, antibodies and ADCs displayed a dose-dependent drug disposition profile in the plasma of NSG mice. The increased clearance rate in NSG mice resulted in the reduction of antitumor activity of ADCs. Furthermore, we identified that the abnormal clearance was mediated by Fc–FcγR interaction by comparing antibodies that lack FcγR binding capacity. We also found a high percentage of FcγR-expressing macrophages in the bone marrow, spleen, and liver of NSG mice, which may be responsible for the abnormal distribution of antibodies. Overall, these findings suggest that preclinical evaluation of efficacy and pharmacokinetics of antibodies and ADCs need to consider mouse strain-induced variations.

Introduction

Monoclonal antibodies have become a major class of therapeutics for cancer patients (1, 2). These include antibodies that modulate oncogenic signaling pathways, kill tumor cells through effector cell functions, activate antitumor immune responses, engage T cells through bispecific targeting, and deliver cytotoxic payloads in the format of antibody–drug conjugates (ADC; refs. 3, 4). There is continued interest to develop novel antibody-based therapeutics, as demonstrated by more than 1,000 active clinical studies evaluating antibodies for cancer treatment (www.clinicaltrials.gov).

Before entering clinical trials, the efficacy and toxicity of antibody drugs are studied in various *in vitro* and *in vivo* models. Most oncology drugs are tested using xenografts, which are implanted in one of the following immuno-deficient mouse strains: athymic nude, severe combined immunodeficiency (SCID), or NOD.Cg-*Prkdc*^{scid}*Il2rg*^{tm1Wjl}/SzJ (NSG; ref. 5). Compared with wild-type mice, these mice lack one or more types of immune cells, allowing the engraftment of foreign tumor cells. Among them, NSG mice are considered the most immune-compromised, because they lack mature T cells, B cells, and natural killer (NK) cells. They also have defective macrophages and dendritic cells due to impaired IL2R signaling. Therefore, NSG mice offer an excellent host for a variety of cancers, especially those of hematologic origin (6).

Despite the successful development of therapeutic antibodies, the mechanisms governing the pharmacokinetics (PK) and pharmacodynamics (PD) of them have not been well elucidated. One of the challenges is that the PK data are often generated in wild type mice or other species of animals (e.g., rat), whereas the PD studies are performed in various immune-deficient mouse strains. Therefore, a direct correlation between the PK and PD would require bridging across different strains of mice or species. Here we examine these potential differences by systematically analyzing the PK properties of antibodies and ADCs across wild-type mice and three immune-deficient mouse strains, to improve the translation between different models.

Materials and Methods

Animal studies

All animal studies were approved by the Seattle Genetics Institutional Animal Care and Use Committee. Balb/c, athymic nude mice, and SCID mice were purchased from Envigo. NOD.Cg-*Prkdc*^{scid}*Il2rg*^{tm1Wjl}/SzJ (NSG) mice were obtained from the Jackson Laboratory (Bar Harbor, ME). NOD/SCID/gamma^{null} (NOG) mice were acquired from Taconic Biosciences. Six- to 8-week-old female mice were used for these studies. For xenograft studies, 5 million cells were implanted subcutaneously and tumor growth was monitored using a digital caliper. Tumor volumes were calculated as $1/2 \times \text{length} \times \text{width}^2$.

A bolus dose of antibody or ADCs was administered via intraperitoneal or intravenous injection for PK studies, whereas the hIVIg was injected intravenously. A total of six animals were injected for each arm of the PK studies. Blood samples were collected using orbital-bleeding techniques, where three of the six animals were collected with a sparse sampling schedule. Terminal cardiac puncture was used to collect blood samples from tumor-bearing animals at the end of study. Plasma was obtained by centrifuging blood samples in Eppendorf tubes containing K2EDTA (BD Bioscience).

[1]Research, Seattle Genetics, Inc., Bothell, Washington. [2]Translational Science, Seattle Genetics, Inc., Bothell, Washington.

Note: Supplementary data for this article are available at Molecular Cancer Therapeutics Online (http://mct.aacrjournals.org/).

Corresponding Author: Fu Li, Seattle Genetics, Inc., 21823 30th Drive SE, Bothell, WA 98021. Phone: 425-527-4626; Fax: 425-527-4609; E-mail: fli@seagen.com

doi: 10.1158/1535-7163.MCT-18-0977

Antibodies, antibody–drug conjugates, and cell lines

Karpas 299 cells were obtained from Dr. Abraham Karpas of the University of Cambridge and were authenticated by IDEXX Laboratories (Columbia, MO). Human intravenous immune globulin injection (hIVIg) was purchased from Grifols Therapeutics. Recombinant hIgG1, αCD30 (clone cAC10) (7), αCD70(clone h1F6) (8), and variants of these antibodies were all produced at Seattle Genetics, Inc. Antibody sequences are included in Supplementary Information.

All antibody–drug conjugates used in this study, including αCD30-vcMMAE, αCD30G1V1-vcMMAE, hIgG1-vcMMAE, hIgG1V1-vcMMAE, and αCD70-mcMMAF were conjugated to average four drugs per antibody at Seattle Genetics, Inc. The conjugation methods were described elsewhere (9, 10).

Radiolabeling

Radioactive antibodies or ADCs were used for most pharmacokinetic studies. The solutions of antibody or ADC containing 500 mmol/L potassium phosphate (pH 8.0) and 500 mmol/L sodium chloride was added to 55 μCi N-succinimidyl propionate, [propionate-2,3-3H]-(Moravek Biochemicals, 80 Ci/mmol, 1 mCi/mL, 9:1 hexane:ethyl acetate solution) per mg of antibody or ADC. The resulting mixture was incubated at room temperature for 2 hours, before it was purified by centrifugal filtration (Amicon Ultra-15 30 kDa MWCO centrifugal filter units; Millipore). The resulting products were further filtered through sterile 0.22 μm Ultrafree-MC Centrifugal Filter Units (Millipore) and the final antibody or ADC concentration was measured. The specific activity (Ci/mg) of each product was determined by liquid scintillation counting.

Radioanalysis

For radiolabeled materials, blood was collected into K2EDTA tubes at various time points. Plasma was isolated by centrifugation for 10 minutes at 10,000 × *g*. A 10 to 20 μL sample of plasma from each time point was added to 4 mL of Ecoscint-A liquid scintillation cocktail (National Diagnostics), and the total radioactivity was measured by liquid scintillation counting. The resulting disintegrations per minute values were converted to μCi, and the specific activity of the radiolabeled test articles was used to calculate the concentration of antibody or ADC remaining in the plasma at each time point.

Enzyme-linked immunosorbent assay

Microtiter plates were coated overnight with a murine IgG1 monoclonal antibody with specificity to human light chain kappa (Jackson ImmunoResearch), or an anti-idiotype monoclonal antibody that binds to αCD30 antibody (Seattle Genetics, Inc.). Samples were diluted into the dynamic range of the assay with naive mouse plasma. Standards, controls, and samples were incubated on the coated and blocked plates. Bound ADCs were detected with horseradish peroxidase-conjugated goat polyclonal antibody reagent with specificity to the Fc region of human IgG (Jackson ImmunoResearch). After incubation and subsequent washing, 3,3′,5,5′ tetramethylbenzidine (ThermoFisher Scientific) was applied to the wells, and the reaction was stopped using 1N hydrogen chloride. The absorbance was measured at OD450 nm using a SPECTRAmax M2 microplate reader (Molecular Devices). Concentrations were then calculated using standards.

Pharmacokinetics analysis

The PK parameters were determined using Phoenix WinNonlin (version 7.0, Certara USA, Inc.). The following PK parameters were determined: area under the plasma concentration–time curve to the last time point (AUC_{last}), maximum observed plasma concentration (C_{max}), time of maximum observed plasma concentration (T_{max}), terminal half-life, clearance (Cl), and calculated volume of distribution at steady-state (V_{ss}). AUC was calculated using the linear log trapezoidal method. Half-lives were reported for plasma concentration–time profiles that had sufficient plasma concentrations in the terminal elimination phase (at least three samples not including T_{max}) and an adjusted R^2 of $\geq$0.8.

Immunohistochemistry

IHC analysis of CD30 on formalin fixed, paraffin embedded tumor sections was performed according to the protocol described previously (11).

Flow cytometry

Mouse liver was dissociated by using Liver Dissociation Kit (Miltenyi) per manufacturer's instructions. Single-cell suspensions from spleen and bone marrow were collected and red blood cells were removed using ACK lysis buffer. Liver tissue were dissociated using GentalMacs Octo dissociator (MACS Miltenyi). Cells were stained with live/dead fixable dye (Invitrogen) to exclude dead cells from analysis. Cell surface antigens were stained with following fluorescence-labeled antibodies: CD45 (30-F11), CD11b (M1/70), Gr1 (RB6-8C5), and F4/80 (BM8). Anti-auristatin antibody was prepared at Seattle Genetics, Inc. Cells were acquired using a Becton Dickinson LSR II flow cytometry and flow cytometric data were analyzed with FlowJo software (TreeStar Software).

Statistical analysis

All analysis performed using unpaired Student *t* test in GraphPad Prism 7.04 software. A *P* value less than 0.05 was considered statistically significant.

Results

Abnormal clearance of antibody-based drugs in the NSG mice

To evaluate whether the mouse strains of xenograft models have any impact on the pharmacokinetics of antibody or ADC, we first measured the plasma concentration of radio-labeled anti-CD30 antibody, αCD30, in four strains of mice: Balb/c, athymic nude, SCID, and NSG. αCD30 is a chimeric IgG1 antibody that recognizes human leukocyte activation marker CD30 (7). Plasma concentrations at 1 hour, 4 hours, 1 day, 3 days, 7 days, and 10 days after dosing were determined using liquid scintillation counting. These measurements revealed that the plasma clearance profiles of αCD30 were comparable in the Balb/c, nude, and SCID mice (Fig. 1A). However, the antibody cleared much faster in the NSG mice, where the clearance rate reached 43.3 mL/day/kg (Fig. 1A; Table 1). Although the half-life of αCD30 was between 7.1 and 16 days in the Balb/c, nude, or SCID mice, it was only 1.4 days in the NSG mice (Table 1).

This observation prompted us to explore whether ADCs have similarly fast clearance kinetics in the NSG mice. A

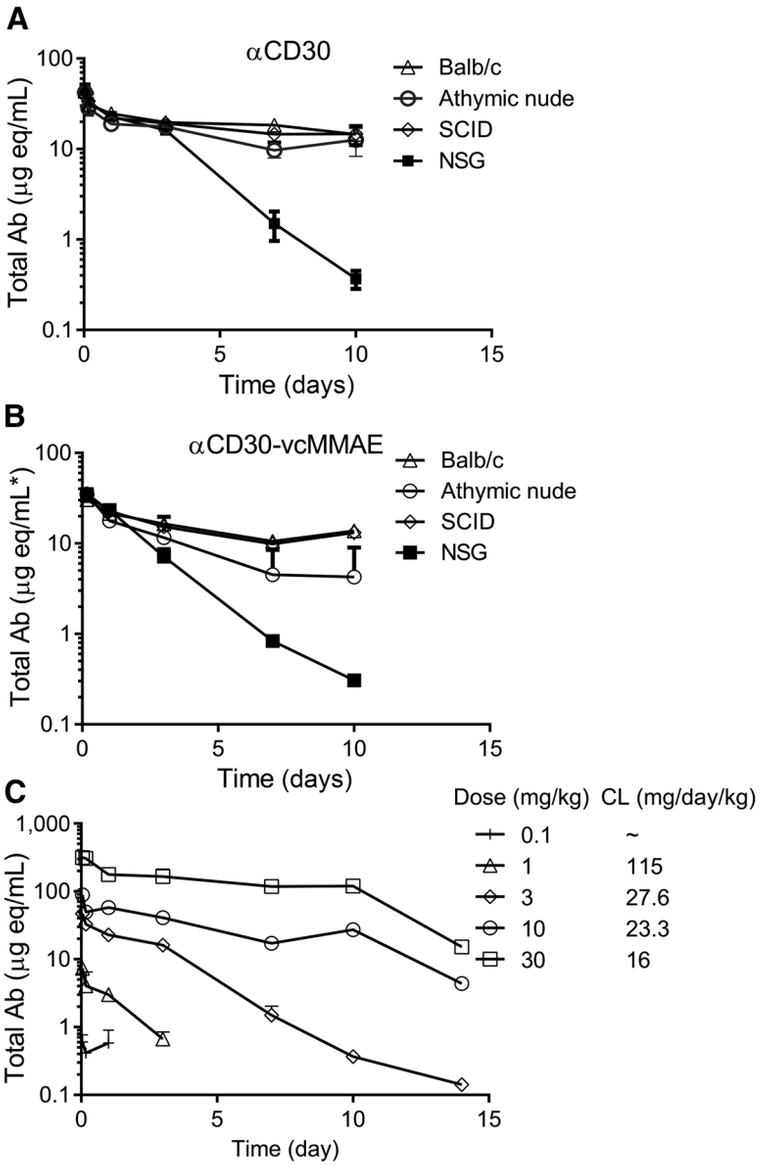

Figure 1.
Plasma concentration of antibody and ADC in various strains of mice. **A,** Mean serum concentrations–time profiles (semi-log scale) of chimeric anti-CD30 antibody following a single 3 mg/kg i.v. injection in Balb/c, athymic nude, SCID, or NSG mice. $n = 3$ per data point. μg eq/mL, equivalent concentration based on radioactivity. Error bar: standard error. $P = 0.001$ comparing NSG with SCID mice using two-way ANOVA test. This experiment was repeated twice. **B,** Mean serum concentrations–time profile of an ADC (αCD30-vcMMAE) following a single 3 mg/kg (i.v.) in Balb/c, athymic nude, SCID, or NSG mice. $n = 3$ per data point. $P < 0.0001$ comparing NSG with SCID mice using two-way ANOVA test. Radioactivity assay was used for this measurement. This experiment was performed twice. **C,** Mean serum concentrations of αCD30-vcMMAE in NSG mice after a single injection at the indicated doses (i.v.). $n = 3$ per time point. Data are measured using radioactive material and LSC counting. CL, clearance. ∼, not determined due to limited data points. This experiment was performed once.

CD30-targeting ADC, αCD30-vcMMAE, was injected into the four strains of mice intravenously at 3 mg/kg (9, 12). In line with the observations of antibody, the ADC also cleared four times faster in the NSG mice than the other strains of mice (Fig. 1B). On average, plasma half-life of the ADC was only 1.4 days in the NSG mice, in contrast to the 6.8 days half-life in the Balb/c mice (Table 1).

Table 1. Pharmacokinetic profile of αCD30-vcMMAE and αCD30 in mice

Strain	AUC_{last} (day/μg/mL)	C_{max} (μg/mL)	Half-life (day)	Cl (mL/day/kg)	V_{ss} (mL/kg)
			αCD30		
Balb/c	113 ± 26	26.4 ± 5.7	7.1 ± 5	16.9 ± 9.4	126 ± 22
Nude	109 ± 28	24.4 ± 1.1	10 ± 10	19.6 ± 16	162 ± 47
SCID	157 ± 14	28.3 ± 4.6	16 ± 8	7.3 ± 3.9	138 ± 4
NSG	67.2 ± 3.6	28.8 ± 2.7	1.4 ± 0.08	44.3 ± 2.5	95.8 ± 11
			αCD30-vcMMAE		
Balb/c	144 ± 22	30.5 ± 5.8	6.8 ± 4	13.8 ± 7.6	116 ± 34
Nude	99.1 ± 35	35.1 ± 1.1	3.7 ± 2	28.6 ± 17	117 ± 20
SCID	149 ± 4.2	35.4 ± 5.8	6.9 ± 0.5	10.9 ± 0.25	124 ± 6.1
NSG	69.9 ± 11	33.4 ± 6.3	1.4 ± 0.1	43.3 ± 7	82 ± 14

NOTE: PK parameters were calculated from data points in Figures 1A and 1B using Phoenix software.
Abbreviations: C_{max}, maximal concentration; Cl, clearance; V_{ss}, the apparent volume of distribution at steady state.
Data shown are mean ± SD.

To rule out whether the abnormal clearance was due to either the unique properties of chimeric αCD30 antibody or the specific biology of the NSG mice, the pharmacokinetic profiles of a humanized IgG1 antibody (αCD70) and an auristatin conjugate (αCD70-mcMMAF) were also assessed in the NOG mice, a highly immune-deficient mouse strain from a different vendor (8, 13, 14). Consistently, both αCD70 and αCD70-mcMMAF cleared rapidly in the NOG mice (Supplementary Fig. S1A).

We then explored whether dose level has impact on the exposure of the antibody in NSG mice. αCD30 was injected at 0.1, 1, 3, 10, or 30 mg/kg, and the plasma concentration measurement is shown in Fig. 1C. The clearance rate decreased as the dose increased, suggesting a nonlinear drug disposition pattern, which saturated between 3 and 10 mg/kg.

Fast clearance reduced ADC efficacy in the NSG mice

To address whether the reduced exposure of antibodies and ADCs in the NSG mice interferes with the efficacy assessment of antibody-based drugs, the αCD30-vcMMAE ADC was studied for its efficacy in the $CD30^+$ Karpas 299 tumors subcutaneously implanted in either SCID or NSG mice (9). The tumor growth kinetics were similar between the two strains, taking approximately 17 days to reach 1,000 mm^3 (Fig. 2A and B). IHC analysis confirmed that Karpas 299 cells retain comparable CD30 expression whether they are in NSG or SCID mice (Fig. 2A and B). We then treated the tumor-bearing mice with αCD30-vcMMAE ADC. In the SCID animals, a single dose of 0.3 mg/kg ADC led to growth delay; and 1 mg/kg ADC resulted in complete remission (Fig. 2C). In contrast, neither of these dosages slowed the growth of tumors implanted in the NSG mice. Moreover, 3 mg/kg ADC could only delay the tumor growth for 10 days (Fig. 2D). These data demonstrate that NSG mice did influence the efficacies of ADCs *in vivo*, presumably due to the reduced exposure.

Fc–FcγR interaction determines the clearance in NSG mice

Because neither αCD30 nor αCD70 antibodies binds murine homologs of CD30 or CD70, we reasoned that the rapid clearance in the NSG mice was mediated through the Fc fragment, but not the Fab domain. Therefore, we studied the

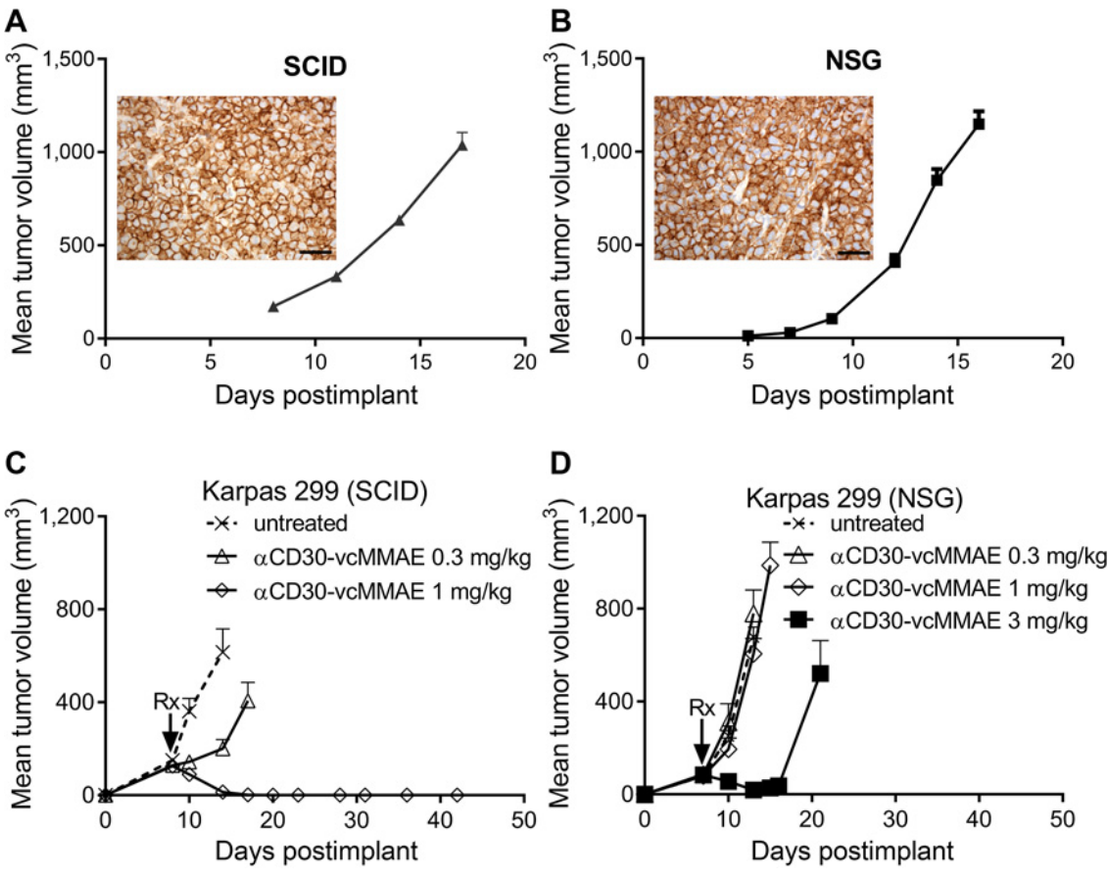

Figure 2.

Responses to ADCs in Karpas 299 xenografts implanted on different host. **A,** Tumor growth kinetics of Karpas 299 cells implanted in SCID mice ($n = 5$). The micrograph indicates uniform CD30 expression as measured by IHC (brown staining). Scale bar: 50 μm. **B,** Tumor growth measurement of Karpas 299 cells when implanted in the NSG mice ($n = 10$). The micrograph depicts CD30 IHC of the tumors grown in NSG mice. Scale bar: 50 μm. **C,** Tumor volume measurement of Karpas 299 xenografts implanted in SCID mice. Tumor-bearing mice received a single intraperitoneal injection of 0.3 or 1 mg/kg of αCD30-vcMMAE. $n = 5$ per group. Rx arrow indicates the date of injection. The experiment was performed twice. **D,** Tumor volume measurement of Karpas 299 xenografts implanted in NSG mice. Tumor-bearing mice received an injection of αCD30-vcMMAE at 0.3, 1, or 3 mg/kg (i.p.). $n = 5$ per group. Rx arrow indicates the date of injection. The experiment was performed once.

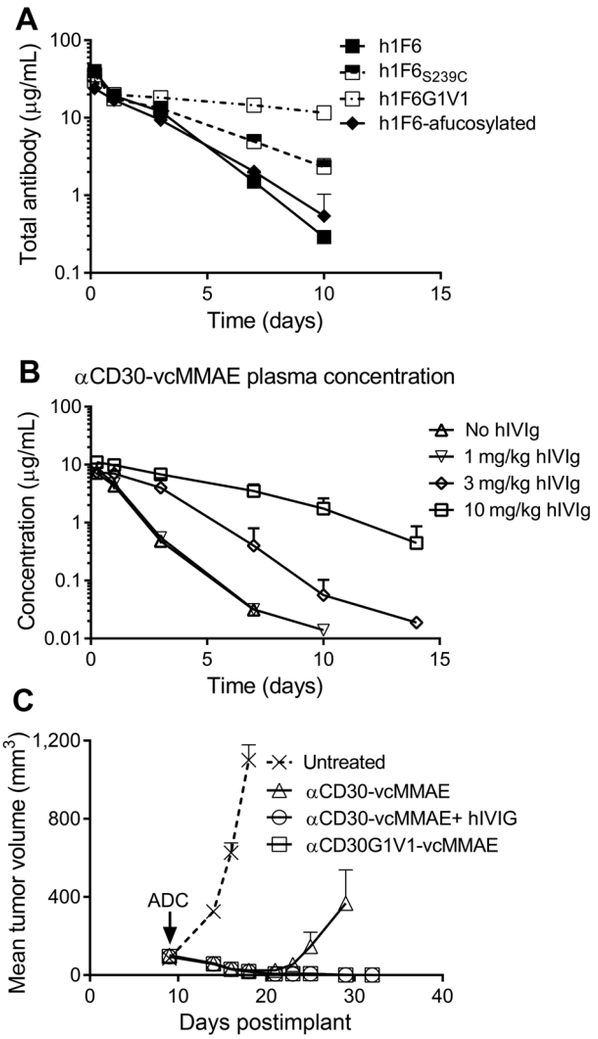

Figure 3.

Roles of Fc-FcγR in antibody pharmacokinetics in NSG mice. **A,** Mean plasma concentration of different CD70 antibodies in NSG mice. All antibodies were injected at 3 mg/kg (i.v.). $n = 3$ per group per time point. The measurement was performed once using radioactive labeling analysis. This experiment was performed once. **B,** Mean plasma concentration of αCD30-vcMMAE after the injection of hIVIg at 0, 1, 3, or 10 mg/kg (i.v.). The hIVIg was injected 24 hours before the ADC administration. ADC was given at 1 m/kg (i.v.). $n = 3$ each point. Plasma concentrations were measured using ELISA. This experiment was performed once. **C,** Mean tumor volume of Karpas 299 xenografts implanted in NSG mice after the treatment of ADCs at 3 mg/kg (i.p.). hIvIg was given at 10 mg/kg (i.v.) 1 day prior to ADC injection when it was injected. $n = 6$ per group. This experiment was performed once.

pharmacokinetics of CD70 antibodies with different Fc interactions: $\alpha CD70_{G1V1}$(E233P:L234V:L235A) lacks the binding to murine FcγRI and FcγRIV; $\alpha CD70_{S239C}$ has reduced binding to FcγRIV, but not FcγRI; and an afucosylated αCD70 has increased affinity to FcγRIV (Supplementary Table S1; refs. 15–17). Surprisingly, $\alpha CD70_{G1V1}$ demonstrated a typical antibody pharmacokinetics profile in the NSG mice. $\alpha CD70_{S239C}$ improved the exposure comparing to the wild-type antibody. In contrast, afucosylated SEA-αCD70 did not reduce the exposure (Fig. 3A). We also compared the PK profile of a recombinant, nontargeting hIgG1-vcMMAE and hIgG1V1-vcMMAE in the NSG mice. Similar to the findings of αCD70 antibodies, ablating FcγRI and FcγRIV interaction with G1V1 mutations also rescued the exposure (Supplementary Fig. S1B). These data suggest that both FcγRI and FcγRIV played a role in the rapid antibody clearance in NSG mice.

We then explored whether excess immunoglobulin supplementation can saturate the abnormal FcγR interaction and, subsequently, increase the exposure the NSG mice. Because 1 g/kg of hIVIg was reported to increase IgG antibody clearance in mice, we selected low dose levels that are unlikely to disturb the FcRn interaction (18). When hIVIg (0, 1, 3, or 10 mg/kg, i.v.) was administered to the NSG mice 24 hours before the αCD30-vcMMAE injection (1 mg/kg, i.p.), the ADC exposure increased following the pretreatment with hIVIg in a dose-dependent manner. Moreover, pretreatment with 10 mg/kg hIVIg was sufficient to restore the half-life of ADC to 7 days in the NSG mice (Fig. 3B).

We then evaluated whether the enhanced exposure by ablating FcγR interaction or saturating with hIVIg could restore the efficacy of αCD30-vcMMAE in the Karpas 299 xenografts in the NSG mice. Remarkably, 3 mg/kg of $\alpha CD30_{G1V1}$-vcMMAE led to complete remissions in this model. Similarly, pretreatment with hIVIg also resulted in complete remissions (Fig. 3C). Further plasma concentration measurement confirmed $\alpha CD30_{G1V1}$-vcMMAE and hIVIg pretreatment have doubled the exposure of αCD30-vcMMAE in the NSG mice (Supplementary Fig. S1C).

Myeloid cells contribute to antibody clearance in the NSG mice

To explore what type of cells may contribute to the abnormal Fc interaction in NSG mice, we focused on the myeloid cell compartment because the NSG mice lack T cells, B cells, and NK cells (6). Flow cytometry analysis revealed a high percentage of bone marrow granulocytic myeloid cells ($CD11b^+Gr1^{high}$) in the immune-deficient SCID and NSG mice, compared with the wild-type Balb/c or nude mice (Fig. 4A). Strikingly, the number of $CD11b^+F4/80^+$ myeloid cells in the bone marrow was 20 times more in the NSG mice when compared with the other strains of mice (Fig. 4B). The high frequency of $CD11b^+F4/80^+$ myeloid cells was also observed in the spleen and liver of NSG mice (Fig. 4C and D). The high abundance of $CD11b^+F4/80^+$ myeloid cells suggest that these cells may mediate antibody clearance in the NSG mice. Indeed, a subpopulation of the $CD11b^+F4/80^+$ cells was found to bind MMAE-conjugated antibody by flow cytometry (Fig. 4E). These data suggest that the myeloid cells in these organs may contribute to the antibody distribution and clearance in the NSG mice.

Discussion

Preclinical PK/PD modeling is widely used in industry to enable the selection and optimization of first-in human doses and regimens, including predicting human efficacious doses (19). However, translating the biological effects between species remain challenging (20). Here we report a unique, rapid clearance phenomenon of therapeutic antibodies in the widely used NSG and NOG mice, where the abnormal clearance reduced antitumor activity of ADC. Importantly, this phenomenon also occurs for several antibodies (chimeric αCD30, humanized αCD70, or nontargeted humanized IgG1). Recently, Sharma and colleagues

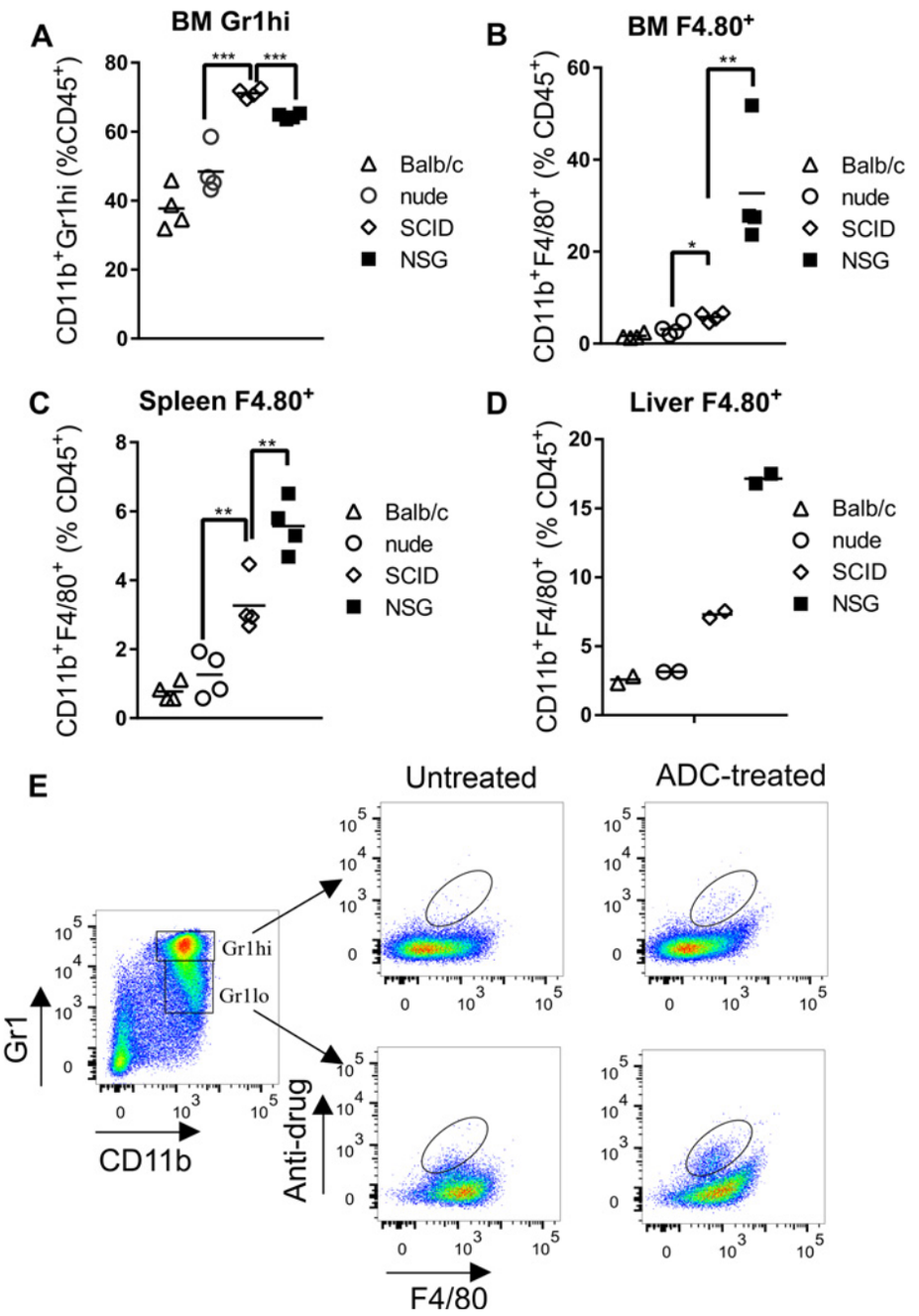

Figure 4.

FcγR-expressing monocytes and macrophages in immune-deficient mice. **A,** Percentage of $CD11b^{+}$, $Gr1^{high}$ neutrophils, and (**B**) monocytic $CD11b^{+}F4/80^{+}$ myeloid cells in the $CD45^{+}$ leukocytes of bone marrow of four strains of mice. $n = 4$ for each group. Percentage of monocytic $CD11b^{+}F4/80^{+}$ myeloid cells in the spleen (**C**) and liver (**D**) of four strains of mice. $n = 4$ for **C**, and $n = 2$ for **D**. *, $P < 0.05$; **, $P < 0.01$; ***, $P < 0.001$, unpaired Student *t* test. **E,** Binding of MMAE-ADC to $F4/80^{+}$ cells in the bone marrow of NSG mice at 72 days posttreatment. Anti-drug antibody detects conjugated MMAE, $n = 3$. This experiment was performed once.

have reported the anomalous biodistribution of trastuzumab and cetuximab in the NSG mice using *in vivo* imaging technology (21). These complementary findings uncover a previously underappreciated role of mouse strains on the preclinical evaluation of therapeutic antibodies. For example, a previous study reported that the advantage of stable drug linker was minimal in a tumor model grown in NSG mice in contrast to the improvement in SCID xenograft model (22). A systematic evaluation of how antibodies, including other subclasses of IgG antibodies, behave across multiple mouse strains may enhance the translation of preclinical PK/PD modeling into human studies.

Multiple mechanisms may influence the pharmacokinetics of therapeutic antibodies and ADCs (23). First, binding to target antigen expressed on certain tissues may cause target-mediated drug disposition. Considering none of the antibodies used in this study are cross-reactive to mouse antigens, the contribution of target-engagement was not examined here. Second, binding with neonatal Fc receptor (FcRn) governs the recycling and half-life of IgG antibodies in circulation (24). Our study indicates a third mechanism may influence the pharmacokinetics of IgG antibodies through interaction with FcγR on myeloid cells. Interestingly, several studies have demonstrated that Fc–FcγR

interaction with tumor-associated macrophages and other antigen-presenting cells may influence the antitumor efficacy of antibody and ADCs in animal models (25–27). However, the contribution of FcγR binding on antibody PK has not been well understood, and it may vary between species (28). Nevertheless, future clinical studies comparing the pharmacokinetics of therapeutic antibodies with altered FcγR and FcRn binding capacity will help elucidate the specific contributions of these receptors in human.

Although researchers tend to choose the most immune-competent mouse strains for preclinical studies, highly immune-deficient strains such as NSG are often required to model human disease. For example, in NOD/SCID mice only a rare fraction of human melanoma cells can establish tumor, in contrast to NSG mice where 25% of melanoma cells can establish tumors (29). Similarly, development of patient-derived xenograft models, particularly those of hematologic origin, has had more success using NSG mice as host (30). More recently, humanized mice derived from NSG mice are adopted to study infectious disease, cancer, graft versus host disease (31). Our study shows that the study of therapeutic antibodies may have been penalized in NSG mouse models, due to the anomalous PK profile. However, one can circumvent the caveat by pretreating mice with hIVIg or using FcγR-mutated antibodies. This study also raises concern on combination studies involving two antibodies in NSG mice, where potential pharmacokinetics changes may confound the results. Nevertheless, with the recent development of transgenic strains containing human FcRn or FcγR genes, NSG mice incorporating these transgenes may serve as better animal models for preclinical evaluation of therapeutic antibodies (32, 33).

Disclosure of Potential Conflicts of Interest

J. Neale is a director at and has ownership interest (including stock, patents, etc.) in Magenta Therapeutics. Dennis R. Benjamin has ownership interest (including stock, patents, etc.) in Seattle Genetics, Inc. No potential conflicts of interest were disclosed by the other authors.

Authors' Contributions

Conception and design: F. Li, V.F.-S. Shih
Development of methodology: V.F.-S. Shih
Acquisition of data (provided animals, acquired and managed patients, provided facilities, etc.): M.L. Ulrich, V.F.-S. Shih, J.H. Cochran, J.H. Hunter, L. Westendorf
Analysis and interpretation of data (e.g., statistical analysis, biostatistics, computational analysis): F. Li, V.F.-S. Shih, J.H. Cochran, J.H. Hunter, J. Neale, D.R. Benjamin
Writing, review, and/or revision of the manuscript: F. Li, V.F.-S. Shih, J.H. Cochran, J.H. Hunter, L. Westendorf, J. Neale, D.R. Benjamin
Administrative, technical, or material support (i.e., reporting or organizing data, constructing databases):
Study supervision: F. Li

Acknowledgments

We appreciate technical help from many colleagues at Seattle Genetics, especially from Devra Olson, Ivan Stone, Cassie Baker Lee, Serena Wo, and Christine O'Day.

The costs of publication of this article were defrayed in part by the payment of page charges. This article must therefore be hereby marked *advertisement* in accordance with 18 U.S.C. Section 1734 solely to indicate this fact.

Received September 5, 2018; revised December 29, 2018; accepted February 20, 2019; published first March 1, 2019.

References

1. Sliwkowski MX, Mellman I. Antibody therapeutics in cancer. Science 2013; 341:1192–8.
2. Kaplon H, Reichert JM. Antibodies to watch in 2018. mAbs 2018;10: 183–203.
3. Redman JM, Hill EM, AlDeghaither D, Weiner LM. Mechanisms of action of therapeutic antibodies for cancer. Mol Immunol 2015;67:28–45.
4. Carter PJ, Lazar GA. Next generation antibody drugs: pursuit of the 'high-hanging fruit'. Nat Rev Drug Discov 2018;17:197–223.
5. Gengenbacher N, Singhal M, Augustin HG. Preclinical mouse solid tumour models: status quo, challenges and perspectives. Nat Rev Cancer 2017;17: 751–65.
6. Shultz LD, Lyons BL, Burzenski LM, Gott B, Chen X, Chaleff S, et al. Human lymphoid and myeloid cell development in NOD/LtSz-scid IL2R gamma null mice engrafted with mobilized human hemopoietic stem cells. J Immunol 2005;174:6477–89.
7. Wahl AF, Klussman K, Thompson JD, Chen JH, Francisco LV, Risdon G, et al. The anti-CD30 monoclonal antibody SGN-30 promotes growth arrest and DNA fragmentation in vitro and affects antitumor activity in models of Hodgkin's disease. Cancer Res 2002;62:3736–42.
8. McEarchern JA, Smith LM, McDonagh CF, Klussman K, Gordon KA, Morris-Tilden CA, et al. Preclinical characterization of SGN-70, a humanized antibody directed against CD70. Clin Cancer Res 2008;14:7763–72.
9. Doronina SO, Toki BE, Torgov MY, Mendelsohn BA, Cerveny CG, Chace DF, et al. Development of potent monoclonal antibody auristatin conjugates for cancer therapy. Nat Biotechnol 2003;21:778–84.
10. Doronina SO, Mendelsohn BA, Bovee TD, Cerveny CG, Alley SC, Meyer DL, et al. Enhanced activity of monomethylauristatin F through monoclonal antibody delivery: effects of linker technology on efficacy and toxicity. Bioconjugate Chem 2006;17:114–24.
11. Li F, Emmerton KK, Jonas M, Zhang X, Miyamoto JB, Setter JR, et al. Intratumoral payload release influences the potency and bystander-killing effects of antibody-drug conjugates in preclinical models. Cancer Res 2016; 76:2710–9.
12. Francisco JA, Cerveny CG, Meyer DL, Mixan BJ, Klussman K, Chace DF, et al. cAC10-vcMMAE, an anti-CD30-monomethyl auristatin E conjugate with potent and selective antitumor activity. Blood 2003;102: 1458–65.
13. Oflazoglu E, Stone IJ, Gordon K, Wood CG, Repasky EA, Grewal IS, et al. Potent anticarcinoma activity of the humanized anti-CD70 antibody h1F6 conjugated to the tubulin inhibitor auristatin via an uncleavable linker. Clin Cancer Res 2008;14:6171–80.
14. Ito M, Hiramatsu H, Kobayashi K, Suzue K, Kawahata M, Hioki K, et al. NOD/SCID/gamma(c)(null) mouse: an excellent recipient mouse model for engraftment of human cells. Blood 2002;100: 3175–82.
15. McDonagh CF, Kim KM, Turcott E, Brown LL, Westendorf L, Feist T, et al. Engineered anti-CD70 antibody-drug conjugate with increased therapeutic index. Mol Cancer Ther 2008;7:2913–23.
16. Sussman D, Westendorf L, Meyer DW, Leiske CI, Anderson M, Okeley NM, et al. Engineered cysteine antibodies: an improved antibody-drug conjugate platform with a novel mechanism of drug-linker stability. Protein Eng Des Sel 2018;31:47–54.
17. Okeley NM, Alley SC, Anderson ME, Boursalian TE, Burke PJ, Emmerton KM, et al. Development of orally active inhibitors of protein and cellular fucosylation. Proc Natl Acad Sci U S A 2013;110:5404–9.
18. Garg A, Balthasar JP. Physiologically-based pharmacokinetic (PBPK) model to predict IgG tissue kinetics in wild-type and FcRn-knockout mice. J Pharmacokinet Pharmacodyn 2007;34:687–709.
19. Nijsen M, Wu F, Bansal L, Bradshaw-Pierce E, Chan JR, Liederer BM, et al. Preclinical QSP modeling in the pharmaceutical industry: an IQ consortium survey examining the current landscape. CPT Pharmacometrics Syst Pharmacol 2018;7:135–46.

20. van der Graaf PH, Benson N. Systems pharmacology: bridging systems biology and pharmacokinetics-pharmacodynamics (PKPD) in drug discovery and development. Pharm Res 2011;28:1460–4.
21. Sharma SK, Chow A, Monette S, Vivier D, Pourat J, Edwards KJ, et al. Fc-mediated anomalous biodistribution of therapeutic antibodies in immunodeficient mouse models. Cancer Res 2018;78:1820–32.
22. Lyon RP, Setter JR, Bovee TD, Doronina SO, Hunter JH, Anderson ME, et al. Self-hydrolyzing maleimides improve the stability and pharmacological properties of antibody-drug conjugates. Nat Biotechnol 2014; 32:1059–62.
23. Ryman JT, Meibohm B. Pharmacokinetics of monoclonal antibodies. CPT Pharmacometrics Syst Pharmacol 2017;6:576–88.
24. Martins JP, Kennedy PJ, Santos HA, Barrias C, Sarmento B. A comprehensive review of the neonatal Fc receptor and its application in drug delivery. Pharmacol Ther 2016;161:22–39.
25. Li F, Ulrich M, Jonas M, Stone IJ, Linares G, Zhang X, et al. Tumor-Associated macrophages can contribute to antitumor activity through FcgammaR-mediated processing of antibody-drug conjugates. Mol Cancer Ther 2017; 16:1347–54.
26. Arlauckas SP, Garris CS, Kohler RH, Kitaoka M, Cuccarese MF, Yang KS, et al. In vivo imaging reveals a tumor-associated macrophage-mediated resistance pathway in anti-PD-1 therapy. Sci Translat Med 2017;9: eaal3604.
27. Waight JD, Chand D, Dietrich S, Gombos R, Horn T, Gonzalez AM, et al. Selective FcgammaR co-engagement on APCs modulates the activity of therapeutic antibodies targeting T cell antigens. Cancer Cell 2018;33: 1033–47.e5.
28. Leabman MK, Meng YG, Kelley RF, DeForge LE, Cowan KJ, Iyer S. Effects of altered FcgammaR binding on antibody pharmacokinetics in cynomolgus monkeys. mAbs 2013;5:896–903.
29. Quintana E, Shackleton M, Sabel MS, Fullen DR, Johnson TM, Morrison SJ. Efficient tumour formation by single human melanoma cells. Nature 2008; 456:593–8.
30. Townsend EC, Murakami MA, Christodoulou A, Christie AL, Koster J, DeSouza TA, et al. The public repository of xenografts enables discovery and randomized phase II-like trials in mice. Cancer Cell 2016;29: 574–86.
31. Walsh NC, Kenney LL, Jangalwe S, Aryee KE, Greiner DL, Brehm MA, et al. Humanized mouse models of clinical disease. Annu Rev Pathol 2017;12: 187–215.
32. Roopenian DC, Christianson GJ, Sproule TJ. Human FcRn transgenic mice for pharmacokinetic evaluation of therapeutic antibodies. Methods Mol Biol 2010;602:93–104.
33. Smith P, DiLillo DJ, Bournazos S, Li F, Ravetch JV. Mouse model recapitulating human Fcgamma receptor structural and functional diversity. Proc Natl Acad Sci U S A 2012;109:6181–6.